Title
NEUTRON EMISSION FOLLOWING u-MESON CAPTURE IN SILVER AND LEAD

Author
Kaplan, Selig N.

Publication Date
1957-04-10

UCRL 3749

UNIVERSITY OF CALIFORNIA

Radiation Laboratory

BERKELEY, CALIFORNIA

DISCLAIMER

UCRL-3749
Physics

UNIVERSITY OF CALIFORNIA

Radiation Laboratory
Berkeley, California

Contract No. W-7405-eng-48

NEUTRON EMISSION FOLLOWING μ-MESON CAPTURE IN SILVER AND LEAD

Selig N. Kaplan

(Ph.D. Thesis)

April 10, 1957

Printed for the U.S. Atomic Energy Commission

Contents

NEUTRON EMISSION FOLLOWING μ-MESON CAPTURE IN SILVER AND LEAD

Selig N. Kaplan

Radiation Laboratory
University of California
Berkeley, California

April 10, 1957

ABSTRACT

The neutron yield from the capture of μ^- mesons in silver and lead has been measured using a high-efficiency Cd-loaded liquid-scintillator tank. The average multiplicities were determined to be: $\bar{\nu}_{Ag} = 1.60 \pm 0.18$, and $\bar{\nu}_{Pb} = 1.64 \pm 0.16$.

The multiplicity distributions were also measured and compared with several theoretical models. Although an α-particle model and a Fermi gas model with neutrons and protons having identical momentum distributions gave results not inconsistent with the data, a Fermi gas model with the effective nucleon mass M^* set equal to $M/2$ seemed to provide the best fit.

I. INTRODUCTION

The μ meson was first recognized as a new subatomic particle a little more than 20 years ago.[1] It was first thought to be the nuclear force quantum predicted by Yukawa,[2] but, as was subsequently shown, it did not have the expected strong interaction with nuclei.[3] At about the time of this latter discovery, the parent π meson was found; this appeared to provide the solution to the Yukawa force problem. Although the μ meson does not interact strongly with nuclei, it does, however, exhibit a weak nuclear interaction, and it is with aspects of this interaction that we shall be concerned.

The μ meson stopping in condensed material is trapped in a Bohr orbit about a nucleus. In a time very short compared to its decay lifetime, it falls into the K orbit[4] (the mesic x-rays predicted to be associated with this effect[5,6] are indeed observed[7]) and from there either decays or interacts with the nucleus.

The now classic experiment of Conversi, Pancini, and Piccioni[3] gave the first evidence of this competition between decay and capture. In later experiments, the μ^- lifetimes were measured over a large spectrum of atomic numbers[8] and they are found to be quite compatible with an interaction of the form of electron K capture, i.e. $\mu^- + Z^A \rightarrow (Z-1)^A + \nu$.[5,9] The nature of the interaction is also verified by experiments designed to observe the reaction products. No photons with energy more than 20 Mev and no electrons are observed;[10,11,12] a very few protons have been observed ($\simeq$ 0.025 per capture in Ag and Br),[13] and it is indicated that one to two neutrons are emitted per interaction.[14,19] These results confirm the interaction assumed above; that is most of the rest energy of the μ meson is carried off in an undetectable way (the neutrino), and the residual nucleus is excited to some 10 to 20 Mev, enough to "boil off" one or two neutrons but not enough to enable many protons to penetrate the Coulomb barrier.

The neutron detection experiments, which are of particular interest to us, may be subdivided into three categories. The earliest experiments in 1948 indicated a correlation between stopping μ mesons

and neutrons.[14, 15] Later work, up to 1951, by the same experimenters and collaborators[16] showed the neutron multiplicities to be at least qualitatively in agreement with the neutrino assumption and the excitation distributions calculated by Tiomno and Wheeler,[20] and Rosenbluth.[21]

However, the third group of experiments, characterized by better statistics and greater neutron-counting efficiencies,[17, 19] seemed to indicate neutron multiplicities about twice as great as were expected on the basis of the theoretical calculations.

If a two-body interaction is assumed, $\mu^- + p \rightarrow n + \nu$, the nuclear-excitation distribution is determined by the proton momentum and energy distribution in the nucleus. The early theoretical work on the problem assumed a nucleon-momentum distribution characteristic of a completely degenerate Fermi gas.[20, 21] Two modifications have been proposed to explain these higher multiplicities. One of these by Lang[22] leaves the momentum distribution unchanged but suggests that $\frac{p^2}{2M}$ be set equal to E/γ (E≡ nucleon kinetic energy), rather than E, where γ is a constant with a value between 1.5 and 2, p is the nucleon momentum, and M is mass. This has the effect of associating a higher energy with a given momentum.

The other proposal, by Cole,[23] suggests modification of the nucleon-momentum distribution to one with a high momentum tail. This distribution is obtained by assuming the initial proton to be part of an α-particle subunit inside the nucleus.

These models can be adjusted to predict the same average number of neutrons but not the same multiplicity distribution. They will be discussed in more detail later in this paper, and their predicted distributions compared with our experimental results.

An excellent review of the experimental and theoretical work on the nuclear interaction of μ mesons through 1952 together with additional references can be found in an article by Sard and Crouch.[24]

This experiment was the result of a proposal by Dr. Edward Teller for a more detailed investigation of nuclear excitation induced by captured μ^-mesons. His interest in the experiment stemmed from

his current work on a nuclear model involving a velocity-dependent potential.[25] The effect of this potential can be interpreted as giving a nucleon a smaller "effective" mass inside the nucleus, smaller by approximately a factor of two. The existence of this effect would modify the nuclear excitation in the manner proposed by Lang (with $\gamma = 2$). Unfortunately, it is very difficult to measure the excitation distribution directly, but we can measure the neutron-multiplicity distribution and then interpret this in terms of a nuclear-excitation distribution.

Previous experiments were unable to yield any useful information in this respect. The most efficient neutron-detection scheme (which was better by a factor of two than any of the others) gave a detection efficiency of only 7%.[19] On the other hand, we had available a large cadmium-loaded liquid-scintillator tank that could be employed in a 4π geometry about a target. In a slightly different application, the tank had exhibited fission-neutron detection efficiencies of as high as 77%.[26] In addition, the large volume of the tank made its efficiency only slightly sensitive to neutron energy over a large range of values.[26]

II. THEORY

After a μ^- meson is absorbed by a nucleus with the accompanying emission of a neutrino ($\mu^- + Z^A \rightarrow (Z-1)^{A*} + \nu$); the excited product nucleus decays primarily by emission of neutrons. A measurement of the number of neutrons emitted following μ^- capture provides a lower limit to the amount of energy imparted to nuclear matter. This limit is the mass difference between the $(Z-1)^A$ nucleus and the Z^A target nucleus plus the binding energies of the observed number of neutrons to the $(Z-1)^A$ product nucleus. The amount of excitation is, in turn, related to the mechanism of the capture and the mutual interactions of the nucleons.

Thus, to make quantitative predictions about the neutron yield from μ^- meson capture, we must first determine the induced nuclear excitation and then relate this excitation to neutron multiplicities.

A. Nuclear Excitation

The nuclear-excitation distribution from μ-meson capture has been estimated by a number of authors.[2-23, 27] The models have the common characteristic of assuming that the meson interacts with a single proton[28] and that the excitation is determined by the assignment of a momentum distribution to the proton and by application of the exclusion principle.

We shall consider:

1. A Fermi gas model (degenerate and nondegenerate)
2. An α-particle model.

1. Fermi gas model

(a) Excitation from degenerate Fermi gas

This model was chosen by previous experimental workers for comparison with their data. It gives a simple and qualitatively plausible kinematic description of the nuclear excitation process. The simplest two-body interaction consistent with conservation of charge, momentum, and energy is assumed, namely, $\mu^- + p \rightarrow n + \nu$.

The μ^- is assumed to be at rest with respect to the center of mass of the nucleus, whereas the proton is given a momentum distribution characteristic of a degenerate Fermi gas.

We shall follow closely the method of Tiomno and Wheeler; however, we shall use more recent values for the numerical constants and consider that the radii of the neutron and proton momentum spheres are different because of the difference in neutron and proton numbers in the nucleus.

Energy conservation may be represented by the expression

$$M_{Z,A} + \mu - B.E._{\mu} = M^*_{(Z-1),A} + p_{\nu}\dagger \qquad (1)$$

where

$M_{Z,A}$	$\equiv$	mass of the target nucleus
μ	$\equiv$	mass of the μ^- meson
$B.E._{\mu}$	$\equiv$	K-shell binding energy of the μ^- meson
$M^*_{(Z-1),A}$	$\equiv$	mass of the excited product nucleus
p_{ν}	$\equiv$	momentum and energy of the neutrino

Because we are attributing the nuclear excitation to the excitation of a single nucleon, we may express the nuclear mass as a core mass (M_c) plus the nucleon energy.

$$\begin{aligned} M_{Z,A} &= M_c + M_p + T'_p - V_p \\ M^*_{Z-1),A} &= M_c + M_n + T'_n - V_n \end{aligned} \qquad (2)$$

where M is the nucleon mass, T' its kinetic energy, $\left(\frac{p^2}{2M}\right)$, and V its potential energy. The subscripts p, n, and ν here and henceforth refer to proton, neutron, and neutrino respectively.

---

†Here and in all of the following discussion we have set $c = 1$, and expressed mass, momentum, and energy in Mev.

If we now assume a Fermi momentum distribution and square well potentials, we may define the difference in ground state energies

$$\Delta M = M_{(Z-1),A} - M_{Z,A} = \frac{P_n^2}{2M_n} - \frac{P_p^2}{2M_p} - (V_n - V_p) + (M_n - M_p) \qquad (3)$$

where P is the momentum radius of the Fermi sphere (Fig. 1). Substitution of Eqs. (2) and (3) into (1) gives

$$\mu' \equiv \mu - B.E._\mu = (T'_n - T'_p) - \left(\frac{P_n^2}{2M_n} - \frac{P_p^2}{2M_p}\right) + \Delta M + p_\nu \qquad (4)$$

or

$$\mu' = \Delta T' - \Delta T + \Delta M + p_\nu$$

where

$$\Delta T' \equiv T'_n - T'_p$$

$$\Delta T \equiv \frac{P_n^2}{2M_n} - \frac{P_p^2}{2M_p}$$

$$= (P_n^2 - P_p^2)/2M$$

(since the effect of n-p mass difference is negligible here).

We may further identify $\Delta T' - \Delta T + \Delta M$ as the total nuclear excitation and, therefore,

$$\Delta T' - \Delta T \equiv Q \qquad (5)$$

as the excitation of the residual nucleus. Thus we may write, finally,

$$\mu'' \equiv \mu' - \Delta M = Q + p_\nu . \qquad (6)$$

Conservation of momentum is expressed by the equation

$$p_n = p_p - p_\nu .$$

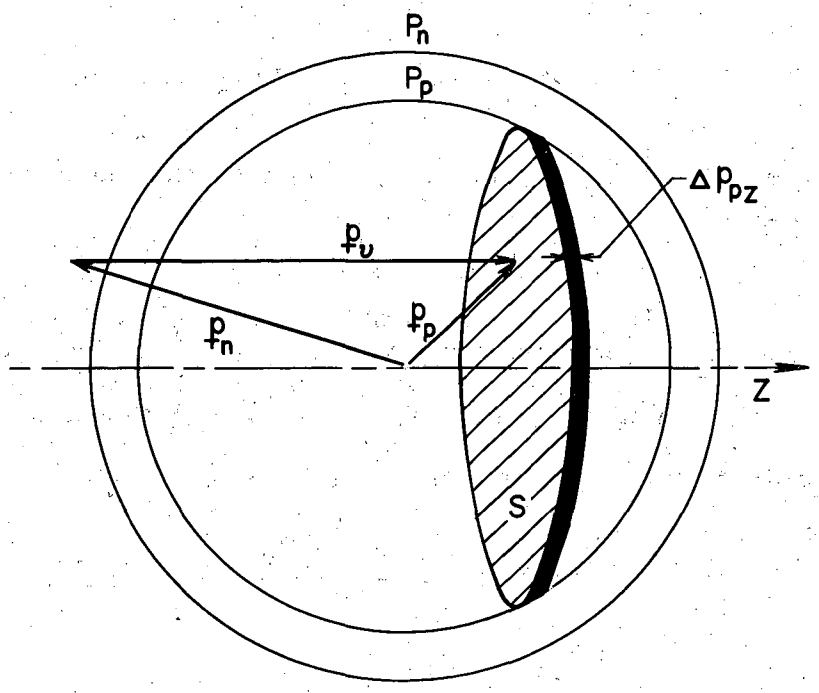

Fig. 1. Relationships of the proton, neutron, and neutrino momenta to the Fermi momentum spheres. The Z axis is defined by the direction of neutrino emission.

Squaring, and noting in Fig. 1 that we have defined the z axis as the direction of emission of the neutrino, we obtain

$$p_n^2 = p_p^2 - 2p_\nu \langle p_p \rangle_z + p_\nu^2$$

$$\frac{p_n^2 - p_p^2}{2M} = \Delta T' = \frac{p_\nu^2 - 2p_\nu \langle p_p \rangle_z}{2M} .$$

Making a substitution from (5) and rearranging terms, we get

$$\langle p_p \rangle_z = p_\nu/2 - M/p_\nu (Q + \Delta T). \tag{7}$$

Note from Eqs. (6) and (7) that Q depends only on the z component of p_p!

The interaction probability is

$$I(Q)\,\Delta Q \propto \left(\begin{array}{l}\text{No. of states in phase}\\ \text{space available to the}\\ \nu + N \text{ system for produc-}\\ \text{ing excitation } Q\end{array}\right) \times \left(\begin{array}{l}\text{No. of protons}\\ \text{in the nucleus}\\ \text{that can lead}\\ \text{to excitation } Q\end{array}\right)$$

Neglecting constant factors, we have

$$I(Q)\,\Delta Q \propto \frac{p_\nu^2\,\Delta p_\nu}{\Delta \mu''} \times S\Delta\langle p_p \rangle_z \tag{8}$$

where S is the area of a slice of the proton momentum sphere normal to the z axis and a distance $\langle p_p \rangle_z$ from the origin. Actually S equals $\pi(R_{max}^2 - R_{min}^2)$, where we must impose an R_{min} to prohibit p_n from falling inside P_n, for this would be a violation of the Pauli principle. Therefore,

$$\begin{aligned} R_{max}^2 &= \langle P_p \rangle^2 - \langle p_p \rangle_z^2 \\ R_{min}^2 &= P_n^2 - (\langle p_p \rangle_z - p_\nu)^2 \end{aligned} \tag{9}$$

Since, from (6), $\Delta p_\nu / \Delta Q \propto$ constant

and, from (6) and (7), $\Delta\langle p_p \rangle_z / \Delta \mu'' \propto \frac{1}{p_\nu}$

we have

$$I(Q) = K_{p_\nu} \left(R^2_{max} - R^2_{min}\right) \quad R^2_{min} > 0$$
$$= K_{p_\nu} \quad R^2_{max} \qquad\qquad R^2_{min} = 0 \tag{10}$$

where K is a normalization constant chosen so that

$$\int_0^{Q_{max}} I(Q)dQ = 1.$$

By substitution of (7) and (9) into (10) we obtain, finally,

$$I(Q) = 2K\, p_\nu\, MQ \qquad\qquad R^2_{min} > 0$$
$$= K_{p_\nu} \left\{ P_p^2 - \left[p_{\nu/2} - M/_{p_\nu} (Q + \Delta T) \right] \right\}, \quad R^2_{min} = 0 \tag{11}$$

with p_ν given by (6).

This excitation distribution is plotted for the case of μ-meson capture in Pb^{208}. We have also plotted equation (11) with $M \rightarrow M/2$. (Henceforth we shall refer to an "effective" nucleon mass M^*). These curves are shown in Fig. 2.

(b) Generalization to nondegenerate Fermi gas

In view of experimental evidence for the existence in lighter nuclei[29] of a high-momentum tail and the possibility that it may also exist in the heavier nuclei, the above calculation has been modified by considering the nucleus to be a Fermi gas, not at 0°, but at a temperature $T = \frac{\theta_F}{k}$, where T is the nuclear temperature in $^\circ K$, k is Boltzmann's constant in Mev/$^\circ K$ and $\therefore$ θ_F is the Fermi temperature of the nucleus (in Mev). In order to so generalize the above calculation, we consider a momentum distribution function $f(p_z)$ such that $f(p_z)dp_z$ is the probability of finding a nucleon with a z component of momentum between p_z and $p_z + dp_z$. We can then redefine (9) by saying:

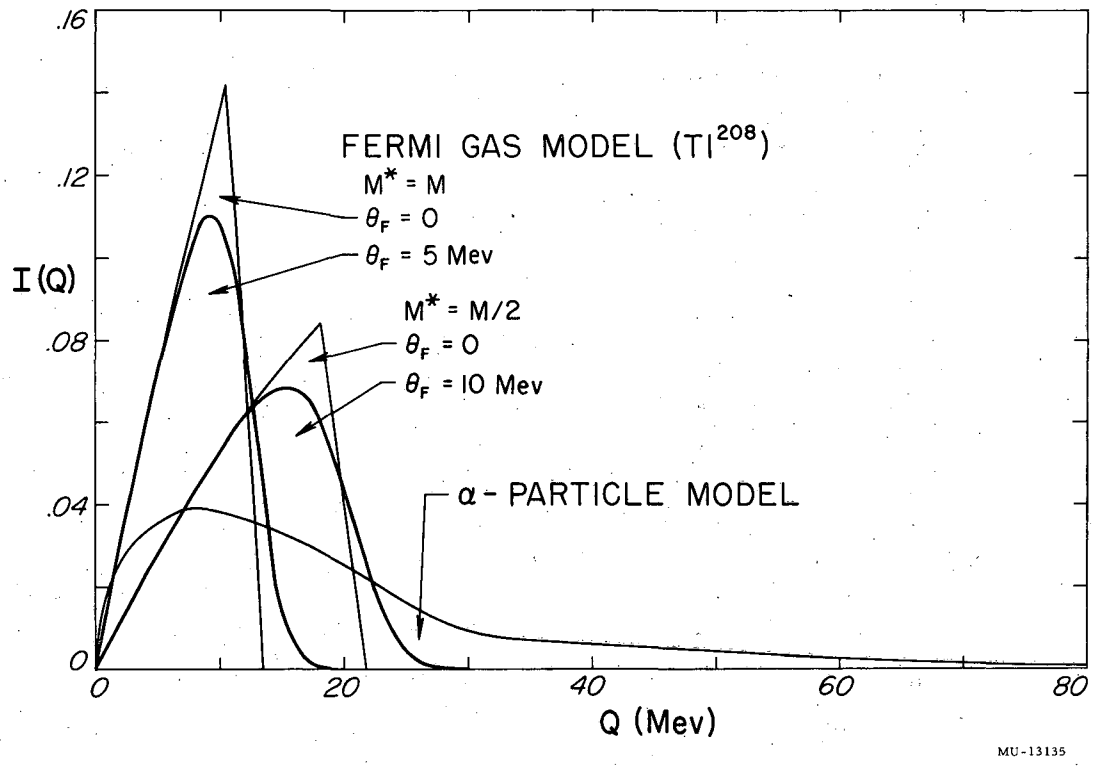

Fig. 2. Nuclear-excitation distributions from μ-meson capture, as predicted by the various theoretical models.

$$R^2_{max} = P_p^2 \left\langle p_p \right\rangle_z^2 \equiv f'\left(\left\langle p_p \right\rangle_z\right) \propto f\left(\left\langle p_p \right\rangle_z\right)$$

$$R^2_{min} = P_n^2 - \left(\left\langle p_p \right\rangle_z - p_\nu\right)^2 = P_n^2 - \left\langle p_n \right\rangle_z^2 \equiv f'\left(\left\langle p_n \right\rangle_z\right) \propto f\left(\left\langle p_n \right\rangle_z\right)$$

where $\left\langle p_n \right\rangle_z$ represents, in this case, the z component of the momentum of that neutron that would have been created by the proton with momentum-z component $\left\langle p_p \right\rangle_z$. Therefore the expression equivalent to (10) is

$$I(Q) = K' p_\nu \left[f'\left(\left\langle p_p \right\rangle_z\right) - f'\left(\left\langle p_n \right\rangle_z\right)\right] \tag{13}$$

with K' chosen so that

$$\int_0^\infty I(Q)\, dQ = 1.$$

The distribution function for a Fermi gas has the form

$$f(|\underline{p}|)\, dp_x\, dp_y dp_z = \frac{1}{N} \frac{dp_x dp_y dp_z}{\exp\left[(p^2 P^2)/2M^* \theta_F\right] + 1}$$

where N is a normalization constant.

We obtain $f(p_z)$ by integrating over all values of p_x and p_y:

$$f(p_z)\, dp_z = \frac{1}{N} dp_z \int_{-\infty}^{\infty} dp_x \int_{-\infty}^{\infty} dp_y \frac{1}{\exp\left[(p_x^2 + p_y^2 + p_z^2 - P^2)/2M^* \theta_F\right] + 1}$$

The integration can be carried out by making the substitution:

$$p_x = p_\rho \cos\phi$$

$$p_y = p_\rho \sin\phi$$

and we get

$$f(p_z) = \frac{\pi \theta_F}{N} \ln \left\{1 + \exp \left[-(p_z^2 - P^2)/2M^* \theta_F\right]\right\}$$

or

$$f'(p_z) = 2M^* \theta_F \ln\left\{1 + \exp\left[-(p_z^2 - P^2)/2M^*\theta_F\right]\right\} \qquad (14)$$

chosen so that $\lim_{\theta_F \to 0} f'(p_z) = P^2 - p_z^2$.

The excitation distribution for a Fermi gas at a temperature θ_F may now be written as

$$I(Q) = 2K'M^*\theta_F\, p_\nu \ln \frac{1 + \exp\left\{\left[P_p^2 - \langle p_p \rangle_z^2\right]/2M^*\theta_F\right\}}{1 + \exp\left\{\left[P_n^2 - (\langle p_p \rangle_z - p_\nu)^2\right]/2M^*\theta_F\right\}} \qquad (15)$$

We have plotted this function (Fig. 2) with θ_F set equal to 5 Mev.[30] A similar curve is shown for $M^* = M/2$ and θ_F equal to 10 Mev. Setting $M^* = M/2$ and leaving p unchanged doubles the nucleon kinetic energy. Because, classically, θ_F is a measure of the average kinetic energy of a collection of particles, it seemed appropriate that a temperature $2\theta_F$ be associated with mass $M^* = M/2$.

2. α-Particle model

The model employed by Cole[23] may be described as follows:

(1) The reaction goes according to the equation

$$\mu^- + He^4 \rightarrow H^3 + n + \nu .$$

(2) As regards momentum conservation, however, only the part $\mu^- + p \rightarrow n + \nu$ is considered.

(3) The proton is considered to be part of the He^4 initially, for the purpose of obtaining a momentum distribution with a high momentum component, and the H^3 in the final state permits application of the exclusion principle.

The energy distribution (I(Q)) is found from first-order time-dependent perturbation theory (Fermi's Golden Rule No. III)[31] with the matrix element obtained from derived wave functions.

This is an artificial model designed to consider in detail the effect on the interaction of neighboring nucleons although neglecting the rest of the nucleus. Emphasizing the effect of the neighboring nucleons allows for higher proton momentum, thus making possible higher energy transfers. The predicted excitation-distribution curve taken from Cole is also shown in Fig. 2.

B. Neutron Emission

In order to interpret the excitation in terms of observed neutron multiplicities, we assume that this excitation, initially in the form of neutron kinetic energy, is quickly shared with other nucleons to produce a "thermally" excited nucleus (the "Bohr assumption").

It was assumed that neutrons were then "boiled off" from the excited nucleus with an energy spectrum of the form:

$$N(\epsilon) \propto \epsilon\, e^{-\epsilon/\Theta}$$ [32, 33]

where ϵ = neutron kinetic energy

Θ = constant that depends upon the nuclear excitation. (For our purposes, we felt it was sufficient to approximate this constant as 0.75 Mev.[32, 33]

The nucleus will continue to emit neutrons until there is not enough excitation left to do so, and only then will it decay to its ground state with the emission of γ radiation. We have assumed the proton emission is negligible.[13, 32]

If the nuclear excitation is in excess of the binding energy of ν neutrons by an amount $\delta_\nu \Theta = Q - B_\nu$, ν or more neutrons will be emitted providing the total kinetic energy of the first ν-1 neutrons does not exceed $\delta_\nu \Theta$, that is

$$\epsilon_1 + \epsilon_2 + \ldots \epsilon_{\nu - 1} \leq \delta_\nu \Theta .$$

The probability of at least ν neutrons being emitted from a nucleus excited to the energy Q can be expressed by the analytical relationship

$$N_\nu \propto \int_0^{\delta_\nu - B_\nu} \epsilon_{\nu-1}\, e^{-\epsilon_{\nu-1}/\Theta} d\epsilon_{\nu-1} \int_0^{\delta_\nu - B_\nu - \epsilon_{\nu-1}} \epsilon_{\nu-2}\, e^{-\epsilon_{\nu-2}/\Theta} d\epsilon_{\nu-2} \int \cdots \int_0^{\delta_\nu - B_\nu - \epsilon_{\nu-1} - \cdots - \epsilon_2} \epsilon_1\, e^{-\epsilon_1/\Theta} d\epsilon_1$$

Integrating this expression and normalizing so that $\lim_{\delta_\nu \to \infty} N_\nu = 1$, we obtain

$$N_\nu = 1 - e^{-\delta_\nu} \sum_{n=0}^{2\nu-3} \delta_\nu^n / n! \qquad (16)$$

where

$$\delta_\nu = \frac{Q - B_\nu}{\Theta}$$

and $B_\nu \equiv$ binding energy of ν neutrons in the original nucleus.

The probability, therefore, of emission of ν neutrons is $N_\nu - N_{\nu+1}$. Figure 3 shows N_ν plotted vs δ_ν for $\nu = 1, 2, 3,$ and 4.

For multiplicities greater than three, as are predicted by Cole's model, we employed his approximation that the number of neutrons emitted from a nucleus excited to an energy Q is proportional to Q,

$$\nu(Q) \propto Q,$$

where the proportionality constant was assumed to be[34]

$$\frac{1}{\frac{1}{2}(B_1 + B_2) + 2}$$

or

$$\nu(Q) = \frac{1}{\frac{1}{2}(B_1 + B_2) + 2}\, Q .$$

We then converted this to a step function with the steps of width $\frac{1}{2}(B_1 + B_2) + 2$.

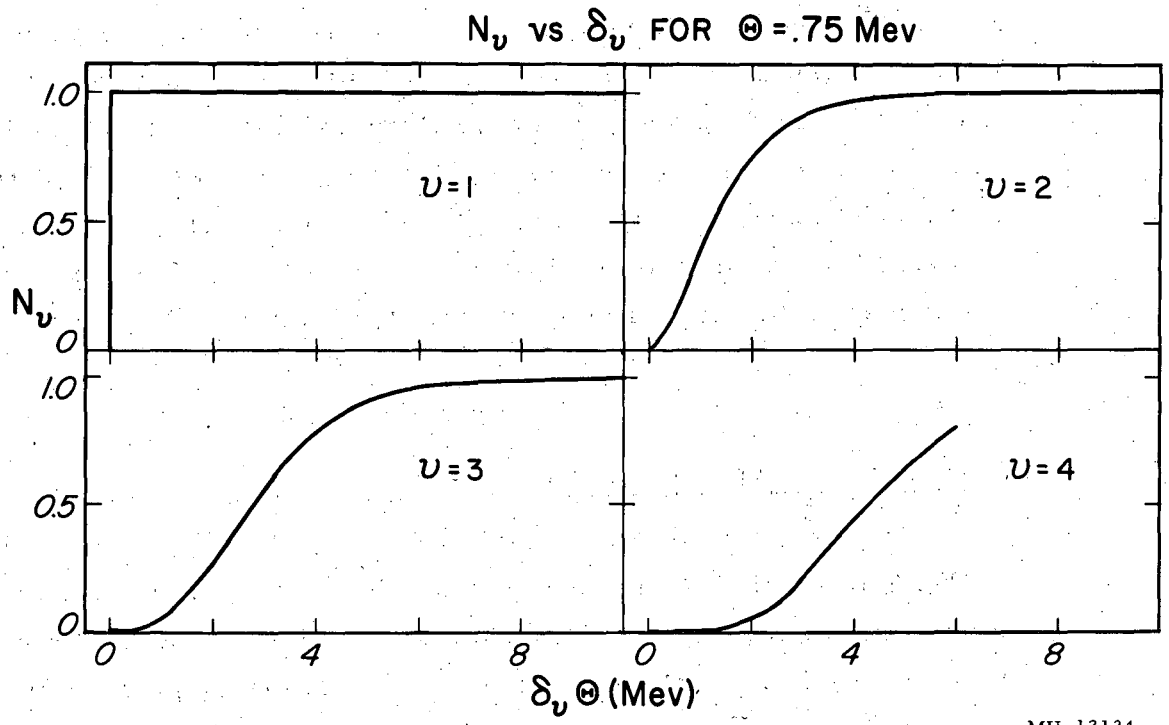

Fig. 3. The probability for the emission of at least ν neutrons versus the nuclear excitation in excess of the binding energy of ν neutrons, $\delta_\nu \Theta = Q - B\nu$.

III. EQUIPMENT AND OPERATION

A. Telescope

The experimental equipment may be considered in two parts--a cosmic ray telescope, and a neutron detector consisting of a large cadmium-loaded liquid scintillator tank. The telescope consisted of four plastic scintillation counters arranged as shown to scale in Fig. 4. A coincidence from Counters I and III triggered the sweeps of two oscilloscopes. On one of the oscilloscopes, A, pulses from Counters II and IV were displayed with appropriated electronic delays in order to show their rise and to separate them on the sweep. With regard to the telescope, the signature of a stopping meson consisted of a triggered sweep on the oscilloscope A, displaying a prompt pulse of the appropriate height from Counter II,[35] but no pulse from Counter IV.

B. Scintillator Tank

1. General physical description

The neutron detector consisted of a tank 30-in. long and 30 in. in diameter with 1/4-in. steel walls.[26, 36] The inside surface was sprayed with a protective coat of molten aluminum and then with a mixture of aluminum oxide abrasive powder,water glass, and water to provide a highly reflective surface. It was filled with a solution of toluene mixed with cadmium propionate dissolved in methanol, p-terphenyl as a scintillator, and a spectrum shifter, POPOP.[37]

The curved surface of the tank has eighty-eight 1/4-inch-thick glass windows each 2-1/8 in. in diameter sealed with neoprene "O" rings. Against each window was mounted a Dumont 6292 photomultiplier tube enclosed in a soft-steel collar. The space between the tube face and the glass was filled with mineral oil in order to make good optical contact. The photomultiplier tubes were wired in parallel in two banks of 44 tubes each, with both banks observing all portions of the scintillator.

A copper electrical shield was placed around the entire phototube assembly, increasing the total diameter to 48 in. Access for the telescope counter and target assembly was provided by an 8-in.-diameter "beam tube" that went completely through the center of the tank. (Fig. 4).

2. Method of neutron detection

Neutrons entering the scintillator are readily thermalized and then captured with a time constant characteristic of the Cd/H ratio. This ratio was set equal to 0.0019 to give a time constant of about 10 μsec. The neutron will be captured by Cd^{113} 95% of the time, giving a cascade γ decay with a total energy of 9.2 Mev,[38] and about 5% of the time it will be captured by H^1, yielding a 2.2 Mev photon. Some fraction of this radiation converts in the tank and gives a pulse indicating the neutron capture.

The sweep circuit of the second oscilloscope, B, was modified so that it swept exponentially, that is, the beam position, x, was proportional to the voltage on a charging condensor. Thus we have $x = x_0 \left[1 - \exp(-t/RC)\right]$, where RC was set approximately equal to 10 μsec, the neutron-capture life time. The sweep was displayed for 30 μsec, or three mean lives. Because of this technique, the neutron pulses were displayed with equal probabilities per unit length of sweep, thereby maximizing the average resolution and making corrections for "pile up" negligible.

3. Additional role of the tank as part of the telescope

Associated with a stopping meson there may or may not have been a prompt tank pulse. (For the case of a stopping μ^- meson, a prompt tank pulse could be caused by the capture X-rays and the radiation emitted by a still-excited nucleus after it was unable to emit further neutrons.)[12] No event was accepted if the prompt tank pulse was higher than the highest neutron pulse, the implication being that the particle was either accompanied by another, or that it scattered into the tank. This is a reasonable assumption because all prompt pulses from the fission calibration, (Section III-C) easily satisfied this pulse-height criterion, and each of them represented the γ

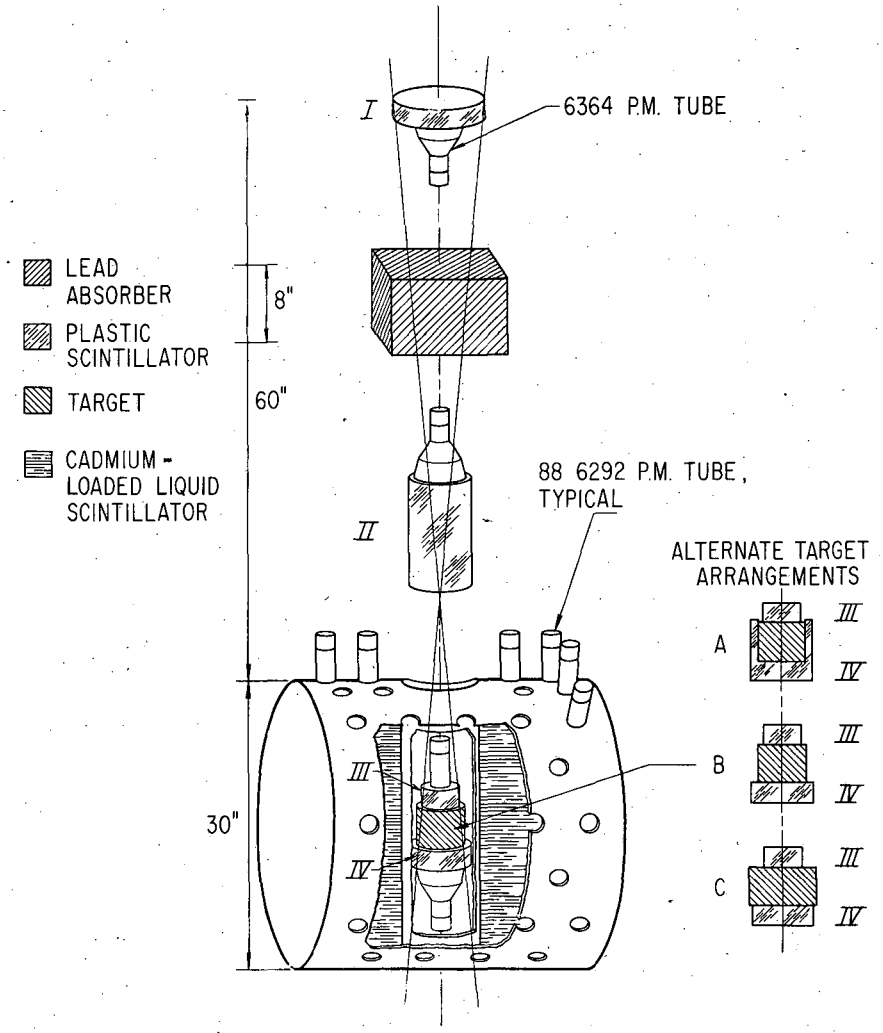

Fig. 4. Experimental counter geometry. A and C represent alternate target arrangements used during part of the Pb run to determine whether any systematic errors could be caused by Coulomb scattering. No such effect was observed.

Further evidence for the absence of such an effect is the good agreement between the observed and calculated relative meson stopping rates in Pb and Ag (Table I).

radiation from two excited nuclei boiling off neutrons. Furthermore during the fission-calibration runs there is little absorbing material present to inhibit this transmission as in the case of γ radiation produced in the lead or silver targets.

Drawings of typical oscilloscope trace pairs produced by a cosmic ray passing through the telescope are shown in Fig. 5. The pairs of traces were recorded on film using a Dumont camera and viewing both scopes by means of a split-mirror arrangement. A complete electronics schematic is shown in Fig. 6.

C. Efficiency Calibration

The neutron detection efficiency of the apparatus was determined with the aid of a sample of the spontaneously fissioning nuclide Cf^{252} in a fission chamber.[26] The telescope counters were disconnected from the circuit, and the oscilloscopes were triggered by the fission-chamber pulse. The fission pulse was displayed on one oscilloscope (Tektronix 545), and the scintillator-tank pulse on the other (Tektronix 517). The primary calibrations were made with Counter III and the target removed and the fission chamber resting on Counter IV. This was done at times of target changing. Every two or three days during the course of the experiment a secondary calibration run was made with Counter III removed and the fission chamber resting on the target (because this was a much simpler mechanical procedure).

The desirability of frequent efficiency calibration was two fold. First, because neutron pulses were counted on the basis of an arbitrarily chosen minimum acceptable pulse height, a change in sensitivity of the system would change the efficiency. This might be caused by a number of things, among them, changes in resistance values in the individual phototube bases and changes in characteristics or complete failure of individual phototubes. Secondly, it has been observed that after several months the cadmium salt begins to come out of solution.[26] This has the effect of decreasing the Cd/H ratio, thereby increasing the neutron-capture lifetime. Because the tank pulses are observed over a constant 30 μsec interval, the detection

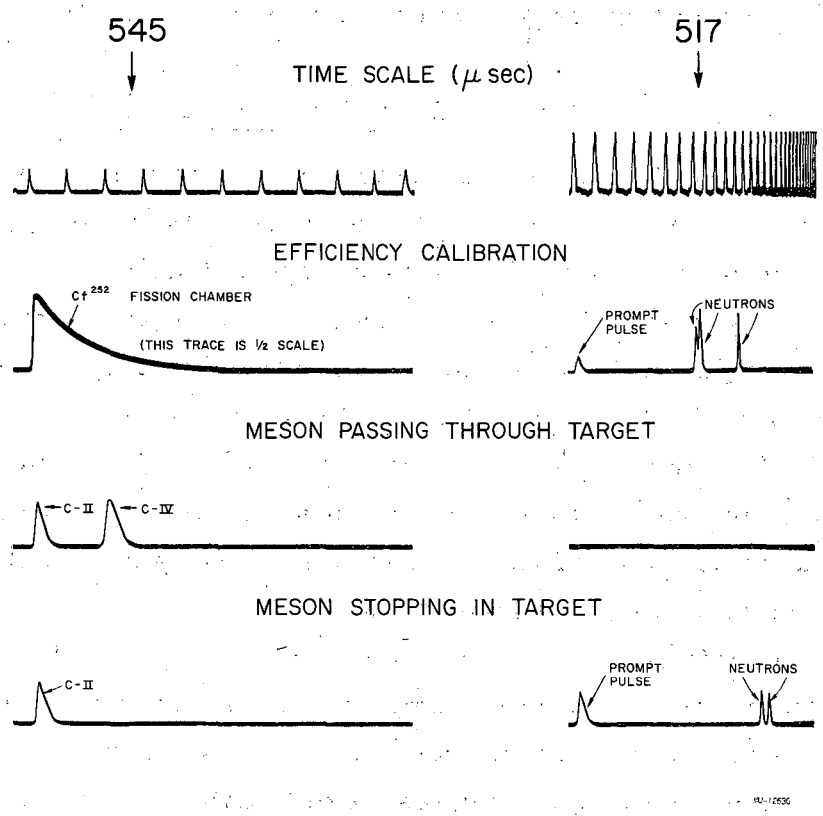

Fig. 5. Typical oscilloscope traces.

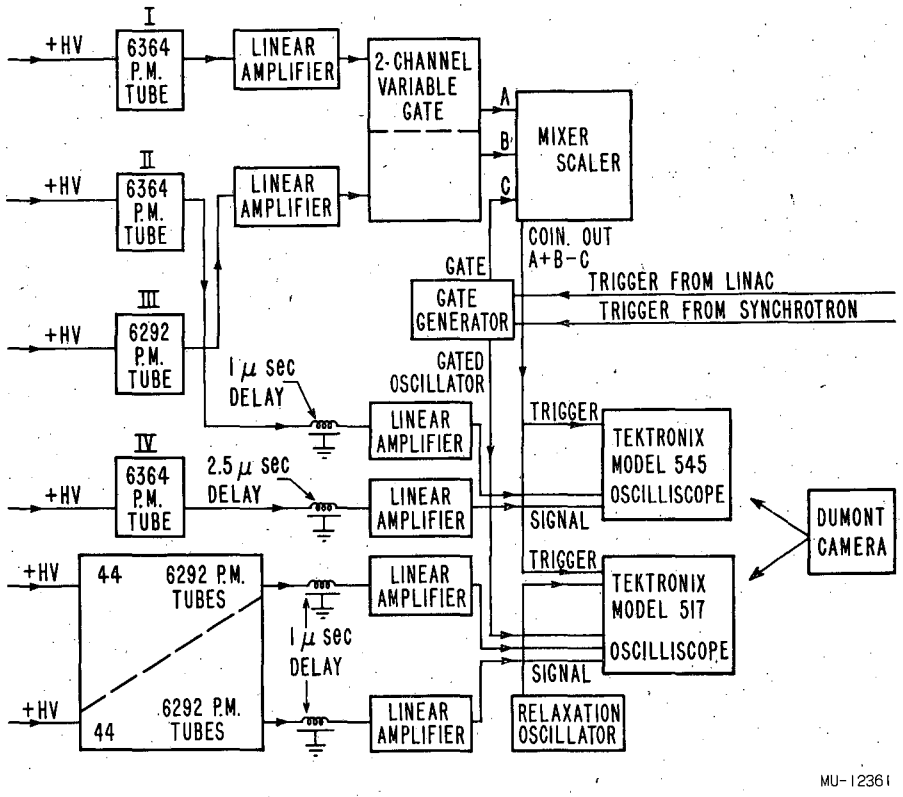

Fig. 6. Block diagram of electronics.

efficiency is decreased. Actually, the detection efficiency decreased from 59% to 51% during the course of the experiment.

D. Equipment Maintenance

The data collection took place over a 200-day period beginning April 20, 1956. The associated equipment was in constant operation except when shut down for repair.

The following stability checks were made:

1. Daily:

(a) The telescope high voltages were checked with an electrostatic voltmeter.

(b) The gains of each of the four telescope counter amplifiers were checked.

(c) Pulses from the four counters were observed on an oscilloscope, and the single counting rates of Counter I and Counter III were checked.

(d) The tank pulse height from each bank was observed when a Na^{22} source was suspended in the beam tube.

2. Every two or three days:

(a) A fission calibration was made.

(b) The high voltages and the amplifier gains of the two tanks were checked.

3. Periodically: (About once a month)

(a) Pulse-height distribution measurements from the film were made for Counter II and Counter IV.

(b) Pulse-height and time-distribution measurements were made from the fission-calibration film.

IV. SOURCES OF ERROR

In interpreting the data, there are several necessary assumptions and corrections that should be mentioned. Since we are not able to identify a particular stopping as a μ^- meson nor a particular tank pulse as a neutron, these identifications must be made statistically.

A. Mesons

1. Contamination of beam

a. Non mu-mesic contamination

We shall first consider the effect on our data of non mu-mesic contamination. Uncharged particles will not trip Counter I. The 8 in. of lead between Counters I and II is quite adequate to eliminate electrons and positrons. (Any conceivable shower event that could partially penetrate and also produce the desired results in Counters II and III would certainly produce an unacceptably large prompt tank pulse). The π-meson flux at sea level is negligible because of the short lifetime of this particle. Therefore, the only contaminants that may be of any consequence are protons. In the energy range of stopping, the P/μ ratio is approximately 0.03.[39] In addition, the absorbing material above Counter III provides almost two mean free paths of attenuation.[39] We have considered the effect on our data by protons to be small but unknown, and no numerical correction has been made.

b. μ^+ mesons

The fraction of stopping mesons that are negative must be calculated from the known μ^+/μ^- ($\equiv r_\pm$) ratio. This was taken to be $r_\pm = 1.21 \pm 0.03$.[40] However, as this appears in the calculation, we have

$$\frac{\mu^-}{\mu^+ + \mu^-} = \frac{1}{r^\pm + 1}$$

$$= \frac{1}{2.21 \pm 0.03},$$

which gives an error negligible compared with the statistical counting error.

2. Fraction of mesons captured

Some of the μ^- mesons decay rather than being captured. The fraction that decays can be determined by comparing the μ^- lifetimes (τ_-) when stopped in lead or silver with the known decay lifetime (τ_d) according to the equation

$$\frac{1}{\tau_-} = \frac{1}{\tau_c} + \frac{1}{\tau_d}$$

where $\tau_c \equiv$ capture lifetime and the fraction that decays before capture equals τ_-/τ_d. The values used in the calculation were $\langle\tau_-\rangle_{Pb} = 0.0745 \pm 0.0083$,[41] $\langle\tau_-\rangle_{Ag} = 0.0844 \pm 0.0035$,[41] and $\tau_d = 2.22 \pm 0.02$,[42] giving $(\tau_-/\tau_d)_{Ag} = 0.038 \pm 0.003$, and $(\tau_-/\tau_d)_{Pb} = 0.034 \pm 0.001$.

B. Neutrons

1. Neutron counting efficiency

The neutron counting efficiency is the product of two functions:

(a) The probability (Eff') that a neutron produced in the center of the beam tube will give a tank pulse.

(b) The probability that the neutron will not be absorbed by the target, that is, the transmission (T).

or

Eff = Eff' x T.

The probability (Eff') is determined by the ratio:

$$\frac{\text{Average no. neutrons observed/Cf}^{252}\text{ fission}}{\text{known average neutron multiplicity from Cf}^{252}\text{ fission}} = \frac{\bar{n}\ \text{Cf}^{252}}{\bar{\nu}\ \text{Cf}^{252}}$$

The value of $\bar{\nu}$ Cf^{252} used in the calculation is 3.869 ± 0.078.[43]

T was determined by measuring the activity induced in a solution of M_nSO_4[44] by a mock-fission[45] neutron source with and without a

target present. In order to simulate the geometry of the scintillator tank, a commercially available galvanized-iron can 30 in. in diameter was filled to a height of 30 inches with the M_nSO_4 solution. In the center of the can, rising vertically, was an 8-in.-diameter iron pipe (the pipe, therefore, was rotated 90^o with respect to the tank dimensions and geometry and those of the can), which was closed at the bottom and weighted down with lead bricks. A hole 1.125 in. in diameter and 2.5 in. deep was drilled in the center of each of the targets to accommodate the 1-in.-diameter by 1-in.-high source. For Pb, the ratio of the target in/target out induced activity was close to unity (0.98 ± 0.02). For Ag, it was smaller, and therefore a third measurement was made, with the source right next to but not inside the target. The measured activity ratios were:

$$\frac{\text{center of target}}{\text{no target}} = 0.87 \pm 0.02$$

$$\frac{\text{side of target}}{\text{no target}} = 0.94 \pm 0.02 \quad .$$

An average transmission for silver was estimated to be 0.91 ± 0.03.

2. Positron contamination

It was also necessary to verify that the tank pulses observed were actually caused by neutrons. In studying these pulses they were divided into two groups; one group included the delayed tank pulses accompanied either by a prompt tank pulse or at least one other delayed pulse (Fig. 7A). The pulses observed here, after being corrected for background, could be explained only as neutrons. Indeed, we see this to be true when we compare their time distribution with that of delayed tank pulses from Cf^{252} fissions. However, if there is no prompt tank pulse, we may still be seeing neutrons (since the radiation accompanying capture may be absorbed in the target), or we may be seeing radiation from positrons from $\mu^+ \rightarrow e^+ + \nu + \nu$ (Fig. 7B.) As can be seen by comparison with Fig. 7A, both of these effects were observed, and a separation has been made on the basis of time distribution. In Fig. 8

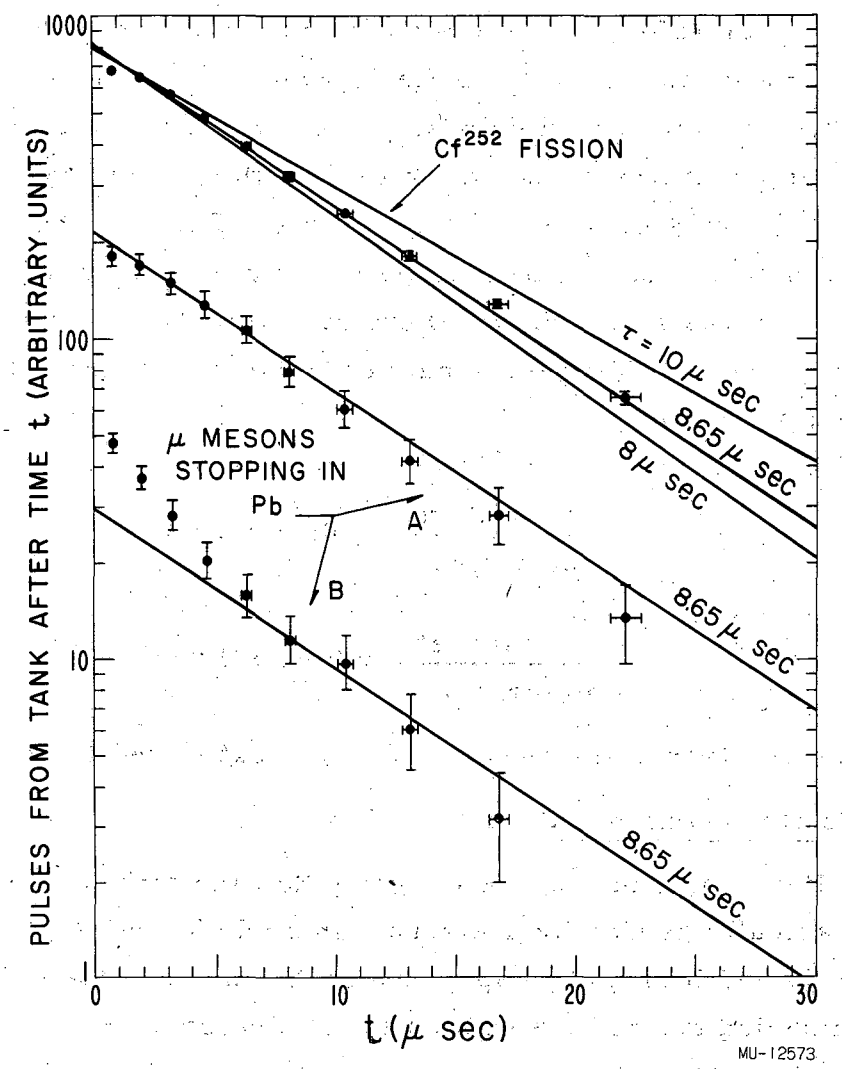

Fig. 7. Time distribution of delayed tank pulses. A is accompanied by at least one other pulse on the sweep, and B is alone on the sweep. The time distribution of pulses from Cf^{252} fission is shown for comparison.

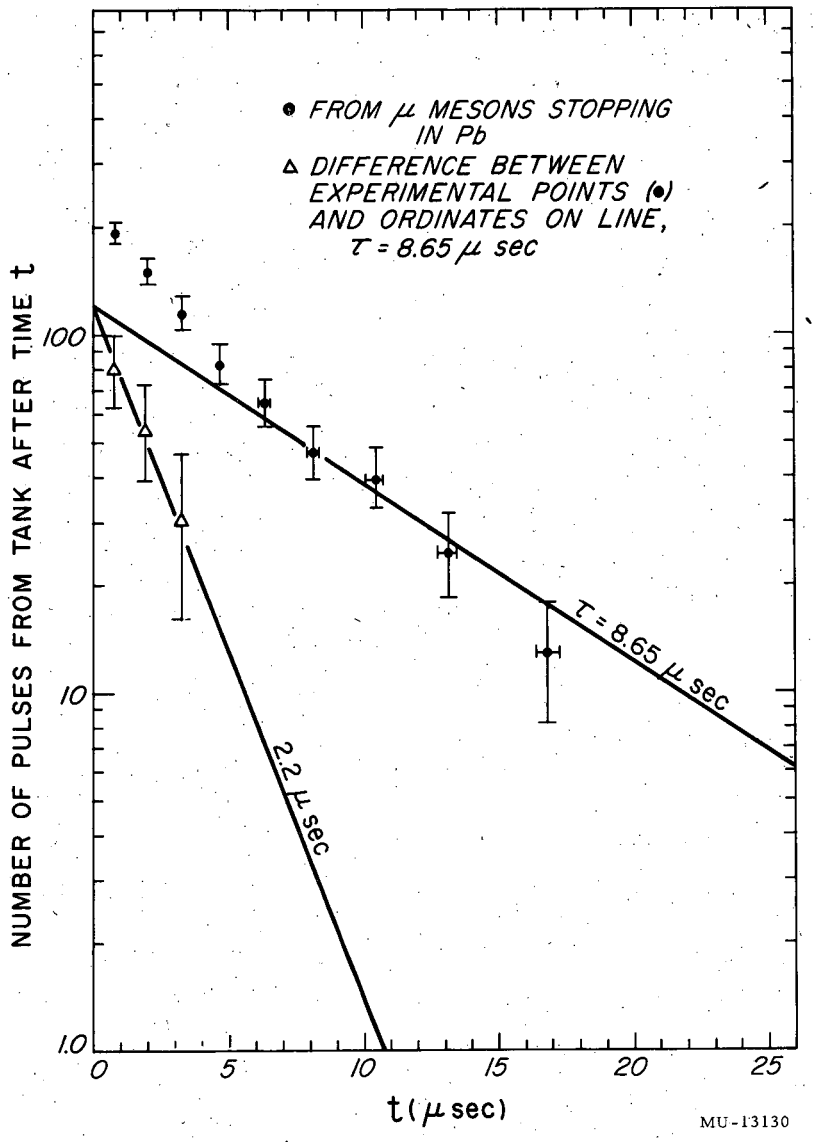

Fig. 8. Separation of μ^+ decay pulses from neutron pulses.

we have replotted the time distribution of delayed tank pulses for cases where they appeared alone on the sweep. The 8.65 μsec neutron lifetime can be "peeled off", leaving a time distribution quite consistent with that for μ^+ decay.

In practice, the correction was made by counting the number of tank pulses for times < 8.1 μsec after the stopping and those for times > 8.1 μsec. The ratio of these was compared with the ratio obtained from the Cf^{252} fissions. The excess pulses for $t < 8.1$ μsec were considered to be due to μ^+ decay.

3. Accidentals

The accidental tank pulses were monitored in two ways. The oscilloscope viewing the tank photomultiplier tubes was triggered by a relaxation oscillator with approximately a 3-min time constant (as compared with the coincident rate of about one every two minutes). The tank pulse rate observed on these artificially triggered sweeps was recorded, and the tank pulse rate observed when a meson passed through the target was also recorded. In both of these cases the rates were found, within statistical error, to be the same, and the pulses were observed to occur randomly in time. Therefore, the pulses associated with a meson passing through the target also represented accidentals. The values used in the calculations were those from the pass-through events. Because the pass-throughs are statistically proportional to the number of stoppings, the average accidental rate for a series of rolls of film could be obtained simply by taking the ratio of the total accidental tank pulses to the total pass-throughs.

V. EXPERIMENTAL RESULTS AND ANALYSIS

A. Results

Before presenting the experimental data, we should explain the choice of targets. Originally, it was intended to perform the experiment on a spectrum of atomic numbers. Four elements were chosen on the basis of a compromise between availability and high density (which, for given dimensions and atomic number, means high stopping power). These elements were Al, Cu, Ag, and Pb. Shortly after the commencement of the experiment, it was decided to concentrate on better statistics for the multiplicity distributions, and hence only the two targets promising the highest neutron yields were used, namely Pb and Ag.

The experimentally determined neutron-multiplicity values together with some other pertinent parameters are tabulated in Table I. The reduced data are given in Table II.

B. Analysis

1. Comparison with theory

The degenerate-Fermi-gas excitation distributions are nearly triangular in shape (Fig. 2). In the calculations these distributions were approximated as triangles with bases defined by the Q axis intercepts and apexes at the Q values of the slope discontinuities. In Fig. 9 an actual curve is compared with the triangle approximation, as are the derived neutron multiplicities. The discrepancy between the average multiplicities derived by triangle approximation and the actual curve is seen to be small compared with the fractional error associated with the observed multiplicity.

In assigning numerical values to the parameters in Eq. (11) and (15), we chose $P_{n(p)}$, the maximum neutron (proton) momentum of the Fermi sphere, from the following relationship in which N(Z) is the number of neutrons (protons):

Table I

Experimentally determined neutron-multiplicity values and other perinent parameters

	Target		
	Pb	Ag	None
Incident beam (total coincidences)	22,842	19,069	21,517
Total stops	909	839	108
Absorbing material in g/cm^2 Pb equiv.*	123.8	135.5	12.3
Relative stops/unit beam	1	1.106	0.114
Relative stopping power (computed)	1	1.095	0.091
Minimum energy to trigger coincidence (Mev)	380	380	380
Corresponding momentum (Mev/c)	475	475	475
Maximum energy to stop (Mev)	525	535	395
Corresponding momentum (Mev/c)	625	635	490
Background pulses/stop	0.064	0.053	0.051
Net efficiency (Eff = Eff'xT)	57.7	50.8	53.6
Tank pulses from μ^+ decays	114 ± 15	134 ± 15	33 ± 6
N_0 (No. of stops with no tank pulse)	512	479	55
N_1 (No. of stops with one tank pulse)	305	293	46
N_2 (No. of stops with two tank pulses)	69	51	4
N_3 (No. of stops with three tank pulses)	14	12	3
N_4 (No. of stops with four tank pulses)	5	2	0
N_5 (No. of stops with five tank pulses)	2	0	0
N_6 (No. of stops with six tank pulses)	1	0	0
N_7 (No. of stops with seven tank pulses)	1	2	0

*The absorbing material included in addition to the targets, a 2-in. plastic scintillator (Counter III); and 0.0625-in. -copper and 0.125-in. -aluminum supporting pieces. The total absorber had an effective stopping power of 12.3 g/cm^2 Pb equivalent.

Table II

Relative neutron multiplicities from μ^- capture

A. In lead (adjusted to 57.7% detection efficiency)

Neutron multiplicity probabilities	Observed	Theoretical					
		Alpha particle	Fermi gas				
			$P_n \neq P_p$			$P_n = P_p$	
			$M^* = M$ $\theta_F = 0$	$M^* = M/2$ $\theta_F = 0$	$M^* = M/2$ $\theta_F = 10$Mev	$M^* = M$ $\theta_F = 0$	$M^* = M$ $\theta_F = 9$Mev
f_0	0.319±0.101	0.325	0.522	0.326	0.331	0.358	0.357
f_1	0.488±0.065	0.363	0.468	0.487	0.469	0.487	0.475
f_2	0.151±0.029	0.181	0.010	0.184	0.184	0.151	0.159
f_3	0.019±0.014	0.078		0.0025	0.016	0.003	0.010
f_4	0.011±0.006	0.032					
f_5	0.006±0.005	0.013					
f_6	0.003±0.003	0.004					
f_7	0.003±0.003	0.001					
Av. neutrons observed per capture $\bar{n}$	0.942±0.089	1.183	0.488	0.863	0.885	0.720	0.795
Av. neutrons emitted per capture $\bar{\nu}$	1.64 ±0.16	2.06	0.845	1.495	1.53	1.25	1.38

Table II (Cont.)

Relative neutron multiplicities from μ^- capture

B. In silver (adjusted to 50.8% detection efficiency)

Neutron multiplicity probabilities	Observed	Theoretical			
		Alpha particle	Fermi gas		
			$P_n \neq P_p$	$P_n = P_p$	
			$M^* = M/2$ $\theta_F = 0$	$M^* = M$ $\theta_F = 0$	$M^* = M$. θ_F=9Mev
f_0	0.415±0.104	0.433	0.353	0.507	0.459
f_1	0.439±0.069	0.362	0.456	0.423	0.451
f_2	0.112±0.026	0.134	0.171	0.069	0.087
f_3	0.025±0.012	0.050	0.020		0.003
f_4	0.003±0.002	0.015			
f_5		0.004			
f_6		0.001			
f_7	0.006±0.004				
Av. neutrons observed per capture $\bar{n}$	0.811±0.088	0.860	0.858	0.564	0.635
Av. neutrons emitted per capture $\bar{\nu}$	1.60±0.18	1.70	1.69	1.11	1.25

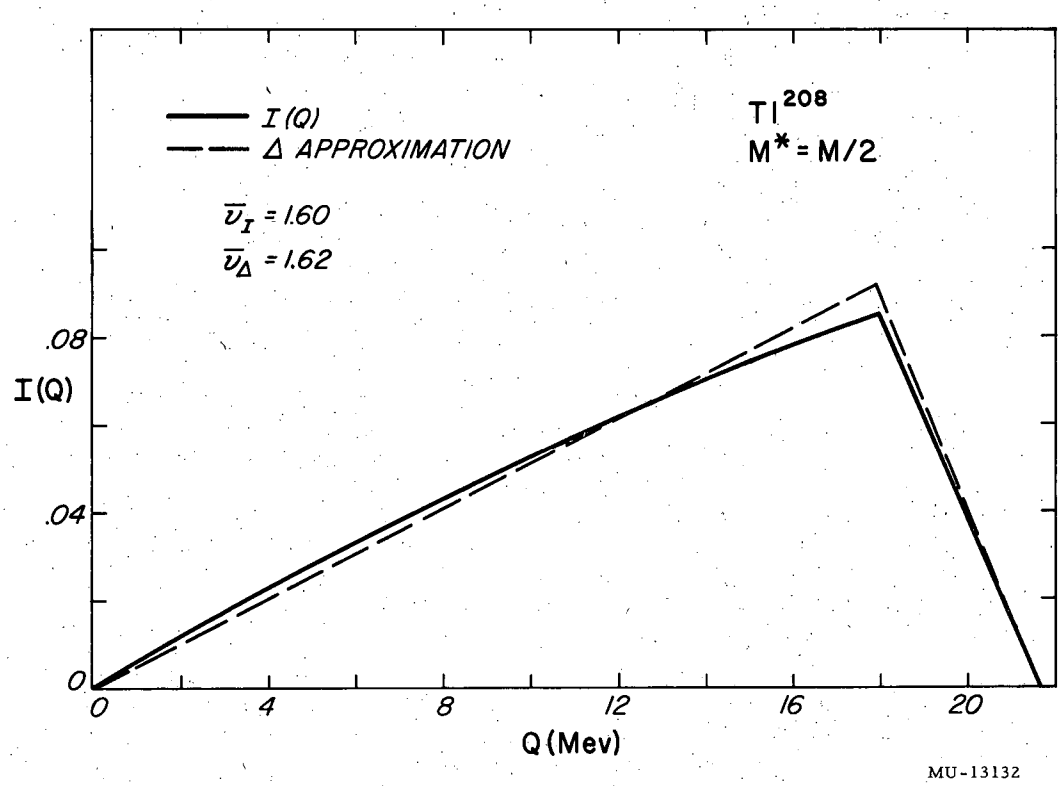

Fig. 9. The excitation distribution of a degenerate Fermi gas compared with a triangle (Δ) approximation used in the calculations.

$$N(Z) = \frac{\text{Spatial volume x momentum volume x 2 (spins)}}{(2\pi\hbar)^3}$$

where the spatial volume is $4/3\ \pi r_0^3\ A$, in which $r_0 = 1.2$ Fermis,[46] and the momentum volume is $4/3\ \pi P_{n(p)}^3$ giving $P_{n(p)} = \frac{\hbar}{r_0}\sqrt[3]{N(Z)\frac{9\pi}{4A}}\ \hbar/r_0$. BE_μ was taken to be 10.5 Mev for Pb and 5 Mev for Ag.[7] The nuclear mass differences, ΔM, are tabulated in Table III.

Integrals of the form $\int_{B_\nu}^{\infty} N_\nu I(Q)dQ$ were evaluated, the probability of emission of ν neutrons, I_ν, being

$$I_\nu = \int_{B_\nu}^{\infty} N_\nu I(Q)dQ - \int_{B_{\nu+1}}^{\infty} N_{\nu+1} I(Q)dQ.$$

For the non-degenrate Fermi gas these integrations were made on the U. C. R. L. differential analyzer, and for the Cole excitation distribution a numerical integration was performed.[47]

The derived values of I_ν were then averaged over the respective natural abundances of the isotopes of Pb[48] and Ag and converted to observation probabilities, f_n. These values, the distributions we would expect to observe having an observation efficiency, ϵ, and actual distributions, I_ν, are expressed by the equation

$$f_n = \sum_{\nu=n}^{\infty} I_\nu\ \epsilon^n (1-\epsilon)^{\nu-n} \binom{\nu}{n}.$$

The calculated values of f_n, tabulated together with the experimental results in Table II, are shown graphically in Fig. 10. Looking at the results for Pb, we see that a degenerate-Fermi-gas model with $M^* = M$ is completely inadequate to explain the multiplicities.

With $M^* = M/2$, the calculated values agree fairly well in the lower multiplicities with those observed. Excitation of the gas to 10 Mev has comparatively little effect on the multiplicities, but it introduces a finite probability for high excitations.

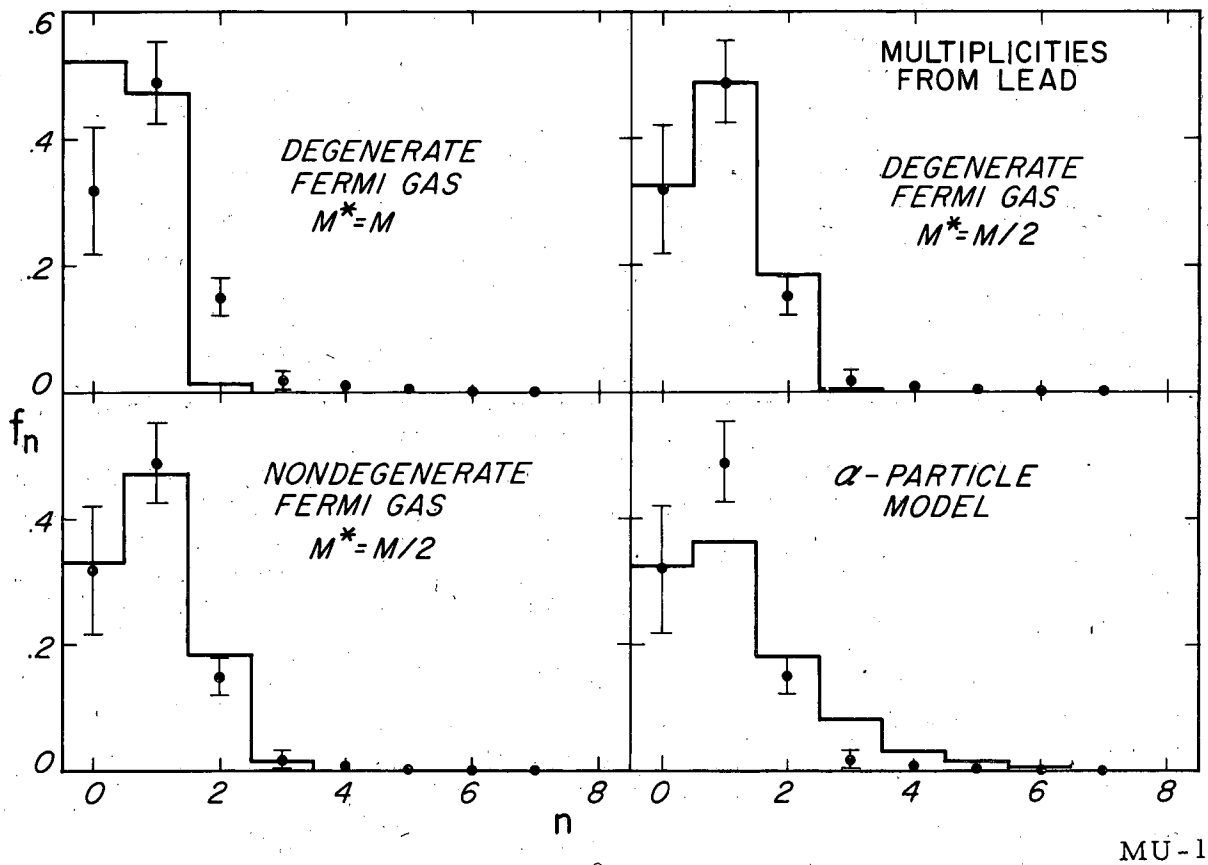

Fig. 10. Comparison of the observed neutron multiplicities from lead with theoretical histograms.

Table III

A. Neutron binding energies

Isotope of Thallium [51]	Binding energy (Mev)	Isotope of Palladium [52]	Binding energy (Mev)
Tl^{208}		Pd^{109}	
	3.86		6.2
Tl^{207}		Pd^{108}	
	6.97		9.1
Tl^{206}		Pd^{107}	
	6.23		6.2
Tl^{205}		Pd^{106}	
	7.48		9.6
Tl^{204}		Pd^{105}	
	6.54		7.1
Tl^{203}		Pd^{104}	
			9.8
		Pd^{103}	

B. Nuclear mass differences [53]

Isotopes	ΔM (Mev)
$Tl^{208} - Pb^{208}$	5.50
$Tl^{207} - Pb^{207}$	1.95
$Tl^{206} - Pb^{206}$	2.02
$Pd^{109} - Ag^{109}$	1.56
$Pd^{107} - Ag^{107}$	0.55

The α-particle model, on the other hand, differs by several standard deviations from experiment for the multiplicities $f_n = 1$ and $f_n = 3$. The observation of the higher multiplicities cannot be explained by the Fermi gas model, whereas the α-particle model predicts more than are observed.

Although one of these two descriptions may provide a distinctly better approximation to the physical situation, the experimental information is not sufficiently complete to allow us to make a clear separation. We are limited by a small but unknown effect of nucleon contamination and a lack of knowledge about the neutron energy spectrum.

In Pb, the number of stoppings accompanied by four or more observed neutrons amounts to only 1% of the total, in Ag to only 0.5%. It would not be unreasonable to assume that this comparatively small fraction of events is caused by proton contamination.[49] From the other point of view, if there are high neutron excitations they will not necessarily always be manifested as large neutron multiplicities. The greater the energy of the produced neutron, the longer will be its mean free path in nuclear matter and, hence, the more likely it will be to leave the nucleus as a high-energy neutron. This effect would tend to increase single neutron emission at the expense of higher multiplicities. Neutrons with energies in excess of 25 Mev have been observed in association with μ-meson capture;[50] however, no quantitative information is presently available.

A comparison of the calculated multiplicity distributions for Ag with those observed gives the same results except at f_2, where the Fermi gas expectation is two standard deviations greater than that observed. (Fig. 11).

It should be noted that in the Fermi gas model used, a higher average neutron multiplicity is predicted for Ag than for Pb. This effect is not observed, but is statistically compatible with the obserations.

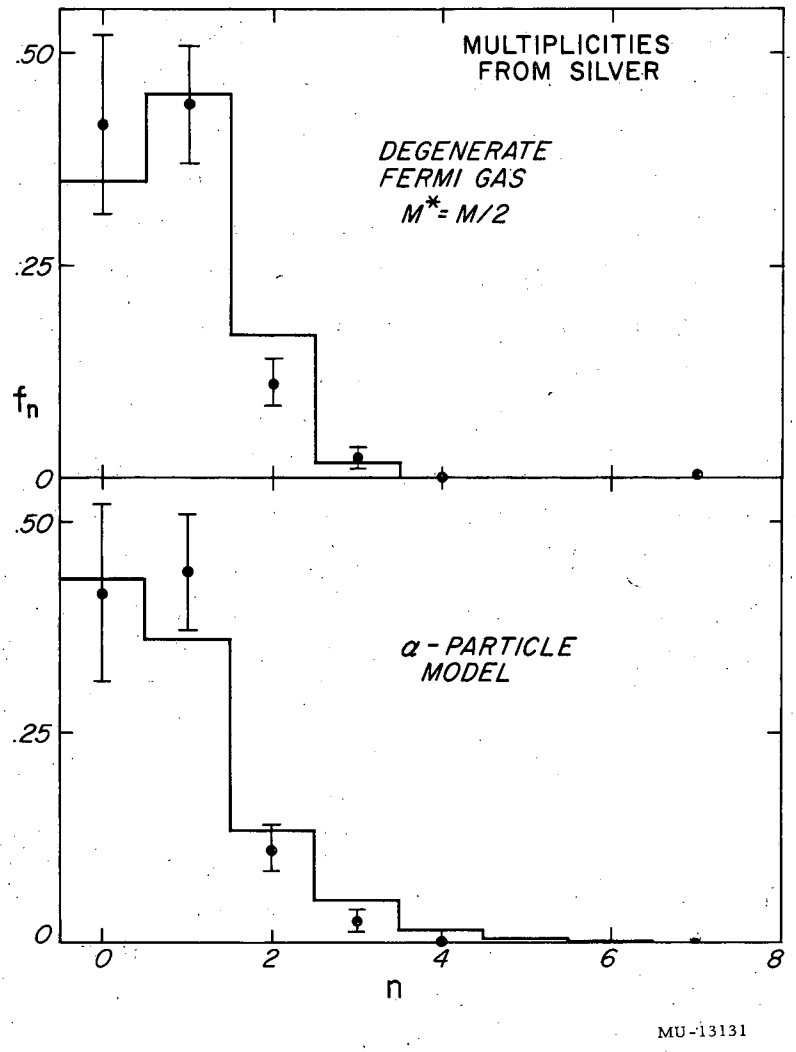

Fig. 11. Comparison of the observed neutron multiplicities from silver with theoretical histograms. The histograms representing a degenerate Fermi gas with $M^* = M$, and a nondegenerate Fermi gas with $M^* = M/2$ have been omitted because the former gave a very poor fit in the case of lead (Fig. 10) and the latter was so similar to that representing the degenerate Fermi gas with $M^* = M/2$.

2. Comparison with other experiments

There are no previous experimental results on the average neutron multiplicities for Ag. The average neutron multiplicities previously reported for Pb are:

University of Chicago	[16]	$\overline{\nu} = 1.96 \pm 0.72$
Washington University	[24]	$\overline{\nu} = 1.7 \pm 0.3$
Cornell University	[19]	$\overline{\nu} = 2.14 \pm 0.13$

The first two results are compatible with ours. However, Widgoff at Cornell obtained a value 30% higher. She does, however, suggest the possibility that there may be a counting efficiency discrepancy of as high as 20% due to the difference between the neutron energy spectrum of capture neutrons and that from a Ra - Be source used for efficiency calibration of her BF_3 counters.

Having available a Ra - Be as well as a mock-fission[45] source, we built a paraffin structure with a rectangular tunnel through the center. (Fig. 12). (This was intended to approximate Widgoff's geometry). A hole large enough to accommodate a BF_3 counter was drilled lengthwise through one of the paraffin blocks forming the structure. By rearranging its position with respect to the other blocks the distance of the BF_3 from the tunnel could be varied, although the counter was always completely imbedded in the paraffin. The neutron counting rate, as a function of distance from the tunnel, was recorded for both sources. The neutron yields were normalized to one another by determining their relative activities with the previously mentioned $MnSO_4$ tank. These results are also plotted in Fig. 12. We see that a descrepancy of as high as 25 to 30% is indicated for a counter 1.5 to 2.5 inches inside the paraffin. (This is where Widgoff's counters appeared to be.)[19] That is, a counter whose efficiency was calibrated at this distance with a Ra - Be source would actually be 25 to 30% more efficient in detecting fission spectrum neutrons. The assumed "boil-off" neutrons would very closely approximate a fission spectrum, which is nothing more than the spectrum of "boil-off" neutrons from the excited fragments.

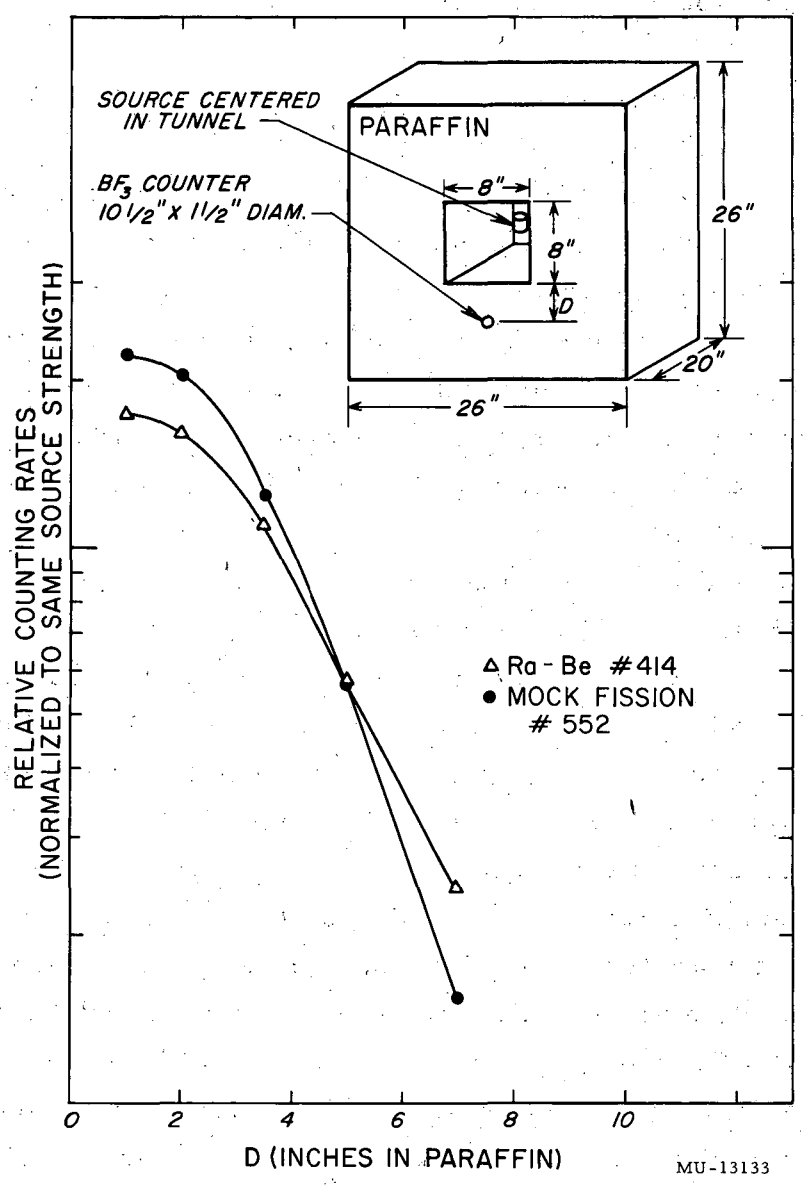

Fig. 12. Relative efficiencies for detection of neutrons from a Ra-Be and a mock fission source. The experimental arrangement was similar to that used by previous experimenters for neutron-detection-efficiency calibrations.

In the theoretical calculations made by the earlier experimenters, it was assumed that $P_n = P_p$. We have reworked these and plotted the results in Fig. 13. (The results have also been worked out for a gas at a Fermi temperature of 9 Mev.) For the degenerate gas, the values calculated by Crouch and Widgoff are $\bar{\nu} = 0.95$ and 0.98, respectively. That our results are so much larger is partially due to our choice of a smaller nuclear proton radius ($R = 1.2\ A\ 1/3 F$ [46]) corresponding to $P_n = P_p \simeq 240$ Mev/c. However, the difference in magnitude results primarily from consideration of the fact that final states from $\mu^- + p \rightarrow n + \nu$ which would leave the product nucleus, $(Z-1)^A$, below its ground state are forbidden. (The introduction of the factor ΔM in the calculation).

We see that the derived multiplicity distribution fits the experimental results quite well, within statistics. However, we note that, even with optimum assumptions with regard to momentum and Fermi temperature, the average multiplicities predicted are considerably more than a standard deviation smaller than the experimental numbers. In view of the large standard errors associated with the experimental multiplicity distributions, it would not be surprising if a large range of curves of the correct general shape (i.e. Fermi gas) did fit the experimental results.

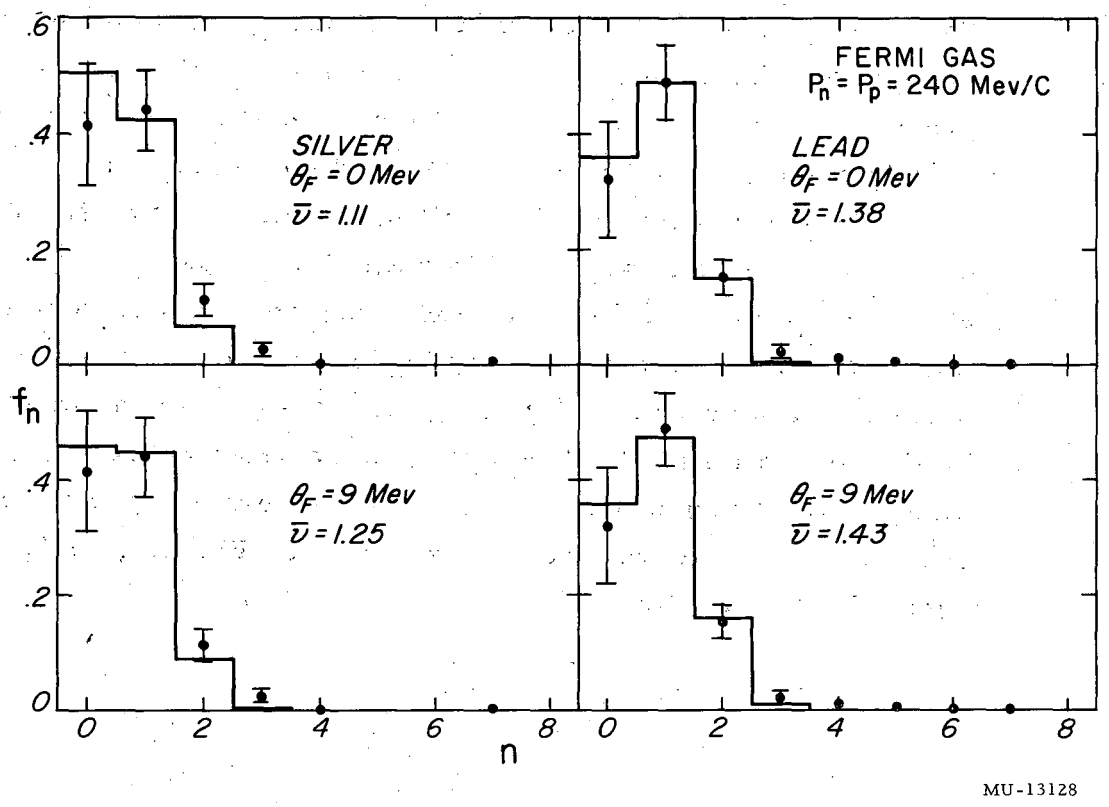

Fig. 13. A comparison of the observed neutron multiplicites with histograms derived from a Fermi gas model assuming the neutron and proton momentum distributions to be the same.

VI. CONCLUSIONS

Upon examination of the neutron multiplicity distribution from μ^--meson capture in heavy nuclei, we obtain results which though not inconsistent with an α-particle model and a Fermi gas model having neutrons and protons characterized by the same momentum distribution, seem to fit best a Fermi gas model with the effective nuclear mass, M^*, set equal to $M/2$. An experiment indicating the virtual absence of multiplicities greater than 4 ($I_\nu << 0.001$) would not only strengthen this point of view but also provide a verification of the assumed interaction mechanism and the nucleon momentum distribution. It should be recognized, however, that the simple models presented here for comparison with the experimental results should really serve only as a guide to more rigorous calculations.

Although we have not been able to make a clear-cut decision as to which type of description best fits the physical reality, we feel that this could be done if better multiplicity data were obtained and more information were available on the neutron energy spectrum.

Repetition of this experiment on the 184-in. cyclotron, when it commences operation, could resolve several of the remaining questions. The use of a well-defined beam of μ^- mesons selected by momentum and range would eliminate the need for correction for contamination by μ^+ mesons, π mesons, and protons. It would then be possible to determine unambiguously whether any large neutron multiplicities are associated with the capture of a μ meson. A more accurate ratio for $\bar{\nu}_{Pb} / \bar{\nu}_{Ag}$ could also be obtained.

VII. ACKNOWLEDGMENTS

The author would like to express his gratitude to the people who helped make this paper possible: Dr. Robert V. Pyle, who was a collaborator throughout the course of the experiment; Dr. George P. Millburn, who did much of the preliminary organization; Professor Burton J. Moyer, who supervised and encouraged this research; and Professor Edward Teller, who first suggested the experiment to Professor Moyer.

He would also like to thank Dr. Warren Heckrotte for many helpful discussions on the theoretical portion. Dr. Francis Cole was kind enough to lend us a personal copy of his thesis for study.

The film was read by Knoxie DeLise and Lucy Lienesch.

Finally, the author would like to thank his wife, who not only typed several preliminary manuscripts, but also painfully copied by hand all the "strange" symbols that were not represented on her typewriter.

This work was performed under the auspices of the U.S. Atomic Energy Commission.

VIII. FOOTNOTES AND REFERENCES

1. S.H. Nedermeyer, and C.D. Anderson, Revs. Mod. Phys. 11, 191 (1939).
2. H. Yukawa, Proc. Phys. Math. Soc. Japan 17, 48 (1935); Revs. Mod. Phys. 21, 474 (1949).
3. M. Conversi, E. Pancini, and O. Piccioni, Phys. Rev. 71, 209 (1947).
4. E. Fermi and E. Teller, Phys. Rev. 72, 399 (1947). See also discussion in R.E. Marshak, Meson Physics (McGraw-Hill, New York, 1952).
5. J.A. Wheeler, Revs. Mod. Phys. 21, 133 (1949).
6. L.N. Cooper, and E.M. Henley Phys. Rev., 92, 801 (1953).
7. V. Fitch, and L.J. Rainwater, Phys. Rev. 92, 789 (1953).
8. H.K. Ticho, Phys. Rev. 74, 1337 (1948);
   Keuffel, Harrison, Godfrey, and Reynolds, Phys. Rev. 87, 942 (1952);
   A. Alberigi-Quaranta and E. Pancini, Nuovo Cimento 11, 607 (1954). A number of other references are given by Sard and Crouch.[23]
9. W.F. Fry, Phys. Rev. 90, 999 (1953). (Direct experimental evidence for the reaction.)
10. J. Steinberger, and H.B. Wolfe, Phys. Rev. 100, 1490 (1955).
11. O. Piccioni, Phys. Rev. 74, 1754 (1948).
12. W.Y. Chang, Revs. Mod. Phys. 21, 166 (1949).
13. H. Morinaga, and W.F. Fry, as quoted by Sard and Crouch;[23]
    H. Morinaga, and W.F. Fry, Nuovo Cimento 10, 308 (1953).
14. Sard, Ittner, Conforto, and Crouch Phys. Rev. 74, 97 (1948).
15. G. Groetzinger, and G.W. McClure, Phys. Rev. 74, 341 (1948).
16. Groetzinger, Berger, and McClure, Phys. Rev. 81, 969 (1951).
17. M.F. Crouch, and R.D. Sard, Phys. Rev. 85, 120 (1952).
18. A.M. Conforto, and R.D. Sard, Phys. Rev. 86, 465 (1952).
19. M. Widgoff, Phys. Rev. 90, 892 (1953).
20. J. Tiomno, and J.A. Wheeler, Revs. Mod. Phys. 21, 153 (1949).

21. M.N. Rosenbluth Phys. Rev. 75, 532 (1949).
22. J.M.B. Lang, Proc. Phys. Soc. (London) A65, 995 (1952).
23. F. Cole, Thesis, Cornell University (1953); also quoted in H. Bethe, and F. de Hoffman, Mesons and Fields, Vol. II, (Row, Peterson and Co., Evanston, Ill., 1956), § 50 d.
24. R.D. Sard, and M.F. Crouch, Progress in Cosmic Ray Physics, Vol. II, (Interscience, New York, 1952), p. 3.
25. M.H. Johnson, and E. Teller Phys. Rev. 98, 783 (1955); H. Duerr, Phys. Rev. 103, 469 (1956).
References in the literature to velocity-dependent potentials actually data back much farther, c.f. J. Bardeen, Phys. Rev. 51, 799 (1937) and Lang.[21] For a different approach to the nuclear force problem that also yields a reduced mass, see K.A. Breukner, Phys. Rev. 97, 1353 (1955); and H.A. Bethe, Phys. Rev. 103, 1353 (1956).
26. Hicks, Lee, and Pyle, Phys. Rev. 101, 1016 (1956).
27. J. Kennedy Phys. Rev. 87, 953 (1952).
28. Tiomno and Wheeler also considered a "dipole model" in which the neutrino is "radiated" from the nucleus as a whole. This model, however, predicts excitations even lower than the single-particle-interaction excitation.
29. Cladis, Hess, and Moyer, Phys. Rev. 87, 425 (1952); J.M. Wilcox and B.J. Moyer, Phys. Rev. 99, 875 (1955).
30. This was an arbitrary choice for illustrative purposes. c.f. L. Rosenfeld Nuclear Forces II, § 12.22, and J. Heideman, Phys. Rev. 80, 171 (1950). As will be seen later, the effect on the multiplicity distribution is small.
31. Orear, Rosenfeld, and Schluter, Nuclear Physics (University of Chicago Press, Chicago, Ill., 1950).
32. J.M. Blatt, and V. Weisskopf, Theoretical Nuclear Physics (John Wiley and Sons New York, N.Y. 1952), Ch. VIII.
33. E.R. Graves, and L. Rosen, Phys. Rev. 89, 343 (1953).

34. Cole argues that the average energy corresponding to the emission of one neutron would be $\simeq 1/2\ (B_1 + B_2)$ if two neutrons were always emitted at B_2. However, because "the neutrons are actually emitted with some kinetic energy (average 1 to 2 Mev), one should add about 2 Mev to $1/2\ (B_1 + B_2)$". Hence we have $1/2\ (B_1 + B_2) + 2$.

35. The pulse-height range was chosen by making a height-distribution measurement of the Counter II pulses for events where the particle also passed through Counter IV (minimum ionization in Counter II). Inclusion of more than 90% of the pulses required a range of acceptance of H of 30% H, where H was the average pulse height, representing a minimum ionization-energy loss of 55 Mev.

36. Reines, Cowan, Harrison, and Carter, Rev. Sci. Inst. 25, 1061 (1954).

37. Hays, Ott, and Ken, Nucleonics 14, No. 1, 42 (1956).

38. G. Bartholomew and B. Kinsey, Phys. Rev. 90, 355 (1953); Can. J. Phys. 31, 1051 (1953); and H. Motz, Phys. Rev. 90, 355 (1953).

39. M.G. Mylroi, and J.G. Wilson, Proc. Phys. Soc. A64, 404 (1951).

40. Robert Brode, private communication.

41. A.J. Meyer, Contract N6CNR-27-II Tech. Rep. No. 16 (NP54/8) Quoted in Nuc. Sci. Abstr. 9-721.

42. W.E. Bell, and E.P. Hinks, Phys. Rev. 84, 1243 (1951).

43. Diven, Martin, Taschek, and Terrell, Phys. Rev. 101, 1012 (1956).

44. A complete descritpion of the $MnSO_4$ technique can be found in G.P. Millburn, UCRL-3320, Thesis (1956).

45. This is a source manufactured commercially by the Mound Laboratories of the Monsanto Chemical Co. It consists of Po, Be, B, Li, and F mixed in proper proportions so that the resultant neutron spectrum resembles that from fission with respect to both average energy and shape.

46. L. Wilets, Phys. Rev. 101, 1805 (1956).

47. This technique gave a value for $\bar{\nu}$ of 2.06 compared to Cole's value of 2.08.

48. Pb^{204}, which is only 1.5% abundant, was neglected in the calculation, and the relative abundances of the other isotopes were adjusted proportionally to give 100%.

49. For example, a 200-Mev proton interacting in Pb may be expected to give an average neutron multiplicity of $\simeq 6$. Cf. W. Crandall, and G. Millburn, UCRL-2706 (1954).

50. V.L. Niklas, and K.H. Lauterjung, Z. Naturforsch. 8A, 214 (1953).

51. J.A. Harvey, Phys. Rev. 81, 353 (1951), (Table II).

52. We were unable to find experimental values for all of these numbers. They were obtained in part from mass value measurements and theoretical values from the following sources: American Inst. of Phys. Handbook (McGraw-Hill New York, N.Y. 1957); B.E. Cushman, UCRL-2468 (1954); and J. Riddell Chalk River Proj. Rept. CRP-654 (1956).

53. Hollander, Perlman, and Seaborg, UCRL-1928 Rev. (1952).